Carbohydrate Polymers 83 (2011) 1696–1706

Contents lists available at ScienceDirect

Carbohydrate Polymers

journal homepage: www.elsevier.com/locate/carbpol

Finite element modelling of crack propagation in carbohydrate extruded starch with open void structure

L. Hedjazi [a], S. Guessasma [a,*], G. Della Valle [a], N. Benseddiq [b]

[a] Research Unit BIA, INRA, Rue de la Géraudière, Nantes 44130, France
[b] Laboratory of Mechanics of Lille (UMR CNRS 8107), University of Lille 1, BP179, 59653 Villeneuve d'Ascq, France

ARTICLE INFO

Article history:
Received 28 July 2010
Received in revised form 20 August 2010
Accepted 13 October 2010
Available online 20 October 2010

Keywords:
Extrusion
Carbohydrate material
Starch
Fracture
Finite element analysis

ABSTRACT

This study presents a new way of describing the void architecture of a of starch foam to allow the simulation of crack propagation in extruded starch material. In these materials, complex stress distribution takes place upon loading leading to a jagged crack extension. Based on the principle of stress intensity factors, the maximum energy release criterion is implemented and combined with a particular 2-D meshing of the material. The meshing is based on a modification of the element connectivity in a regular grid. A material property is assigned to each element based on grey level of acquired images of the carbohydrate material. The numerical results show that the void structure is responsible for the development of a local mixed mode. Crack propagation exhibits significant changes in the crack path because of the heterogeneous stress distribution. The comparison between numerical and observed crack paths well shows that the predictions are sensitive to grey level distributions and mesh refinement. Finally, the criterion is able to predict nicely the crack extension if the contrast between bright and dark regions is properly addressed.

1. Introduction

Extrusion is a popular way of food processing (Guy, 2001; Ho, Karwe, & Kokini, 1991) allowing the design of food products with a wide diversity of textures and formulations, such as breakfast, snacks. Starch is the basic ingredient in such products. Its extrusion leads to the creation of a foam solid as a result of the expansion during processing (Babin, Della Valle, Dendievel, Lourdin, & Salvo, 2007). The resulting void architecture of the carbohydrate polymer depends on the processing conditions and, in turn, significantly affects the texture of the designed product (Babin et al., 2007; Wilkinson, Dijksterhuis, & Minekusy, 2000). One of the targeted functional properties is the size reduction of the product during mastication (Lucas, Prinz, Agrawal, & Bruce, 2002; Voon, Lucas, Chew, & Luke, 1986). Such feature is intimately related to the texture of the food product and undoubtedly to its mechanical properties. There was a considerable effort dedicated to the study of the relation between the mechanical properties of the designed food and the mastication performance (Dan & Kohyama, 2007). Finite element computation also has been considered for the study of the oral (i.e., physiology of mastication) process (Dejak, Mlotkowski, & Romanowicz, 2003; Rohrle & Pullan, 2007). These studies are, however, limited to the analysis of the stress state in teeth and jaws for particular loading conditions (Ichim, Kieser, & Swain, 2007; Reina, Garcıa-Aznar, Domınguez, & Doblare, 2007).

More importantly, the mechanical behaviour of the chewed product is either completely ignored or roughly approximated in several approaches (Okada, Honma, Nomura, & Yamada, 2007; Turker, Sowman, Tuncer, Tucker, & Brinkworth, 2007; Xu et al., 2007). For example, macroscopic homogeneity of the mechanical properties is often assumed but we know that the food transformation process induces a complex structure with a non-homogeneous distribution of mechanical properties.

A better understanding of food failure under real mastication conditions would certainly require a deeper analysis of the rupture of the studied carbohydrate material. There is a huge body of work in that area, within a more general context related to the mechanics of cellular materials. In our specific case, the cell structure refers to the highly porous starch material.

One of the most known result is that the compression behaviour of the cellular material is quite different from its tensile behaviour (Gibson & Ashby, 1997). For the former one, the deformation mechanism is basically determined by the crushing of cells. This mechanism can be approached using linear elastic fracture mechanics. If the material rupture is brittle, the rupture can be anticipated using single crack growth.

This hypothesis is not quite restrictive in the context of mastication. Several studies show that food compression results in

* Corresponding author. Tel.: +33 (0)2 40 67 50 36; fax: +33 (0)2 40 67 51 67.
E-mail address: sofiane.guessasma@nantes.inra.fr (S. Guessasma).

0144-8617/$ – see front matter © 2010 Elsevier Ltd. All rights reserved.
doi:10.1016/j.carbpol.2010.10.031

significant bending of the food part and consequently to the development of an opening mode (Dejak et al., 2003; Lucas et al., 2002).

In such a way, the fracture behaviour of cellular food products was also studied (Babin et al., 2007; Fontanet, Davidou, Dacremont, & LeMeste, 1997; Kirby & Smith, 1998; Primo-Martin, de Beukelaer, Hamer, & van Vliet, 2008; Sandoval, Chaunier, Courcoux, & Della Valle, 2008). One of the major result is related to the effect of the void ratio ϕ on the critical stress intensity factor (Gibson & Ashby, 1997):

$$K_{IC} \propto \sigma_{fs} \rho^n \quad (1)$$

where K_{IC} is the critical stress intensity factor (the fracture toughness), σ_{fs} is the fracture stress of the intrinsic material composing the cell wall, $\rho = 1 - \phi$ is the relative density. n is an exponent equal to 1.5, for a regular array of cells.

Choi and Sankar (2005) report values for n in the range 0.79–1.1 depending on the cell length and strut thickness using numerical simulations.

Eq. (1) has a more general validity and does not prejudge of the nature of the cellular material. However, this equation considers only a microstructure descriptor as affecting a mechanical property. And even so, the property is expected to vary by the action of other descriptors such as cell wall size distribution, variability of the wall properties, among other effects.

The fracture toughness in Eq. (1) determines when a crack is expected to propagate under given loading conditions. However, it is not informative about the crack trajectory unless to consider adequate criteria that combine the stress state around the crack tip and the elastic energy expression using Hook's law. Crack trajectory is related to the fragmentation stage in the mastication process, and thus requires a particular attention.

Within this context, a finite element approach is developed to account for the explicit effect of the void structure of extruded starch on the crack propagation.

Crack propagation has been widely studied, but we focus, in the following, on the literature dealing with the topic of heterogeneous materials where unstable crack growth is microstructural dependent. The most available literature on this topic concerns randomly structured materials such as concrete, fibrous and particulate composites (Bazant, 1997; Guarino, Garcimartin, & Ciliberto, 1998; Jenq & Shah, 1988). The topic of cellular materials has also covered the fracture mechanics (Choi & Sankar, 2005; Schmidt & Fleck, 2001; Thuvander, Jernkvist, & Gunnars, 2000) but with more focus on fatigue failure analysis (Ingraham, DeMaria, Issen, & Morrison, 2009; Kanny, Mahfuz, Carlsson, Thomas, & Jeelani, 2002; Motz, Friedl, & Pippan, 2005; Vendra, Neville, & Rabiei, 2009), damage (Lipperman, Ryvkin, & Fuchs, 2007a; Taylor, Hazenberg, & Lee, 2003; Wittel, Dill-Langer, & Kroplin, 2005) and crack propagation criteria (Dillard, Forest, & Ienny, 2006).

From the computational viewpoint, crack propagation has been studied in random materials using lattice or discrete element models (Belytschko, Organ, & Gerlach, 2000; Schlangen & Garboczi, 1996, 1997; Wittel et al., 2005). The main principle behind is the discretisation of the material by means of 1-D elements (in a 2-D microstructure) that exchange forces and can be thus eliminated when a given criterion is satisfied. Such method is mesh dependent and the results are considerably dependent on the fracture criterion. Finite element computation was extensively used for the study of unstable crack propagation. Damage based approaches such as cohesive models have been implemented (Cornec, Scheider, & Schwalbe, 2003; Gasser & Holzapfel, 2005; Wu & Yin, 2003). The technique is able to cope with stress singularity considering a few number of parameters that can be adjusted based on experimental observation (Cendon, Galvez, Elices, & Planas, 2000). The success of the cohesive model is based on the choice of the traction–separation law, but the model remains phenomenological. Some refinement of the method has been introduced based on a cohesive interaction law that accounts for nonlinearities and surface energy effects in nanomaterials (Gao & Ji, 2003). Micromechanical models have been used to determine the failure of heterogeneous materials by knowing the spatial distribution of mesoscale heterogeneity (Thuvander et al., 2000; Zhu & Tang, 2004). Other finite element approaches are more based on damage formulation (Geers, de Borst, & Peerlings, 2000). Finally, efficient techniques exploiting computer graphics such as cellular automata were also considered for the simulation of 3D crack patterns (Gobron & Chiba, 2001).

The heterogeneous structure has a significant effect on the crack propagation. Size effects have been identified leading for example to the concept of crack fractality (Bazant, 1997; Morel, Bouchaud, Schmittbuhl, & Valentin, 2002). Fracture toughness in cellular materials is, in this way, dependent on the cell size (Gibson & Ashby, 1997). Size effects introduce a limitation in the study of crack propagation in cellular materials. Indeed, the analysis of the discrete cell rupture using continuum mechanics supposes that the crack length is some order of magnitude larger than the cell size.

In this paper, crack propagation in starch porous material is studied accounting for the following developments:

- In our finite element model, we assign to each element material properties based on the observed grey level associated with the void structure of starch material. This principle is used in several computational approaches aiming at implementing material properties related to some information about the heterogeneous microstructure (Chiaia, Vervuurt, & VanMier, 1997; Prado & van Mier, 2003; Thuvander et al., 2000; Zhu & Tang, 2004). This technique contrasts with the approaches using the description of cellular materials as regular assemblies of beam elements (Choi & Sankar, 2005; Lipperman, Ryvkin, & Fuchs, 2007b; Ryvkin, Fuchs, Lipperman, & Kucherov, 2004; Schmidt & Fleck, 2001).
- We use a regular meshing combined with a specific element connectivity to avoid extensive computation with remehsing. Our technique allows thus a non-prescribed crack propagation with no need to special interface elements (Alfaiate, Pires, & Martins, 1997).
- We use the stress intensity factors to derive our crack growth criterion. These have proved to be applicable in several cellular food products (Vincent, 2004). Among the possible criteria, we use the maximum energy release criterion.

2. Experimental layout

The raw material is a maize starch prepared using two high amylose content starches following the procedure detailed in Della Valle, Colonna, Patria, and Vergnes (1996), Della Valle, Vergnes, Colonna, and Patria (1997). The final amylose content is 47% for the material denoted B in the same work (Della Valle et al., 1997).

The material is processed using a Clextral BC45 twin-screw extruder (screw diameter 56 mm, screw length 1 m). The processing conditions are fixed as follows: screw rotation speed 166 rpm, feed rate 33.4 kg/h, added water during feeding 27.5%. Under these conditions, the product temperature in the die channel is 167 °C, whereas the specific mechanical energy is 167 Wh/kg. More details about the processing procedure can be found in Babin et al. (2007), Della Valle et al. (1996) and Della Valle et al. (1997). The final moisture of the extruded material is adjusted to 12% thanks to long duration storage under a controlled environment (relative humidity 60% over saturated NaBr salt and temperature 20°). Samples, regular in shape, of dimensions 30 mm × 10 mm × t mm are carefully machined using a circular saw (thickness = 0.1 mm) from the extruded ribbons for mechanical testing, where t is the material

thickness varying between 1.4 and 3.0 mm. The relative density of the material is 0.30 as indicated by the measured densities of the dense (ρ = 1400 kg/m^3) and the extruded (ρ = 420 kg/m^3) materials. The overall void content of the material is thus about 70%.

Mechanical testing is undertaken using a micro-mechanical testing machine capable of micro level displacement. The load cell has a peak force of ±125 N with an accuracy of 0.25 N. The driving system is composed of two synchronised motors ensuring a displacement accuracy of 1.25 μm. Traction is performed on notched specimens. Samples are fixed by a drop of super glue onto the fixtures. The gauge length is adjusted to about 10 mm (Fig. 1a).

Tensile loading is performed at a constant displacement rate of 40 μm s^{-1} and up to material failure. Mechanical testing is coupled to image acquisition using a digital camera with a recording rate of 100 frames per seconds. The frame size is adjusted to allow sample observation with a fine resolution and as large as possible Region Of Interest (ROI). For this purpose, the digital camera is mounted on stereomicroscope (Fig. 1b). Fig. 1a shows the dimensions of the ROI as well as the loading conditions. Typically, for a ROI of 10 mm length, the pixel size is about 33 μm.

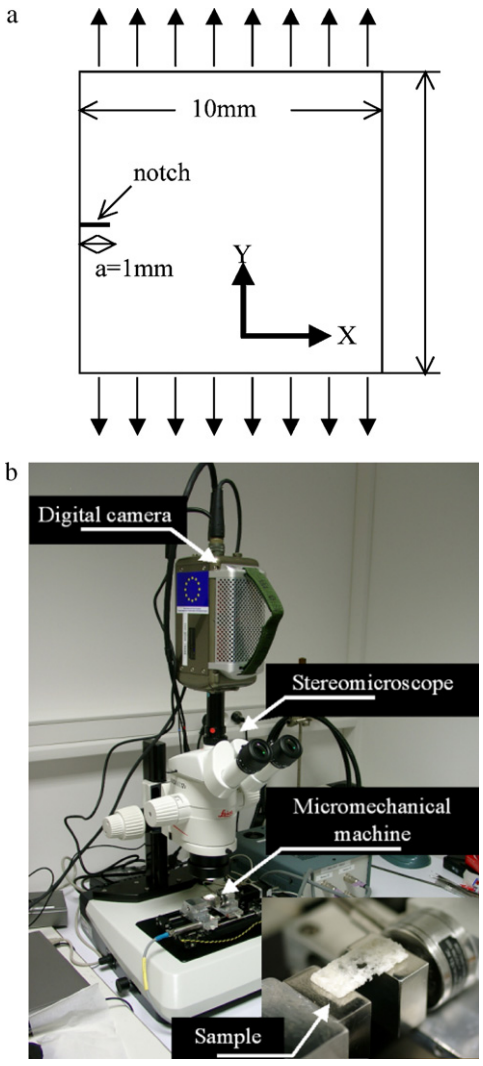

Fig. 1. (a) Dimensions of the observed ROI of the carbohydrate polymer showing in particular the notch size for tensile loading experiment and (b) experimental set-up for tensile loading of extruded samples.

3. Numerical technique

3.1. Crack propagation criterion

In order to define the crack propagation criterion for the studied carbohydrate polymer, we use the concept of the J integral (Gdoutos, 2005) introduced by Rice (1968). Following the definition of the J integral in the case of a mixed mode analysis (Saouma, 2008):

$$J_1 = \int_{\Omega} \left[\Gamma \, dy - t \frac{\partial u}{\partial x} \right] ds \tag{2}$$

$$J_2 = \int_{\Omega} \left[\Gamma \, dx - t \frac{\partial u}{\partial y} \right] ds \tag{3}$$

where Ω is a contour surrounding the two-dimensional crack. Γ is the strain energy density, u is the displacement vector, t is the traction vector along the unit vector n, which is perpendicular to the path defined by the contour.

J_1 and J_2 represent the energy release rate for crack extensions parallel and perpendicular to the crack.

Expressing the two contour integrals as function of stress intensity factors leads to the following relationships:

$$J_1 = \alpha \left(K_{\mathrm{I}}^2 + K_{\mathrm{II}}^2 \right) \tag{4}$$

and

$$J_2 = 2\alpha K_{\mathrm{I}} K_{\mathrm{II}} \tag{5}$$

with

$$\alpha = \frac{1}{E} \quad \text{for plane strain} \tag{6a}$$

and

$$\alpha = \frac{1 - \nu^2}{E} \quad \text{for plane stress} \tag{6b}$$

where E and ν are Young's modulus and Poisson coefficient, respectively. K_{I} and K_{II} are the stress intensity factors associated with the opening and shearing modes.

The corresponding angle of propagation can be thus defined by the ratio of the energy release rates parallel and perpendicular to the crack (Hellen & Blackburn, 1975). It can be thus written as

$$\theta = \arctan \left(\frac{J_2}{J_1} \right) \tag{7}$$

which simplifies into

$$\theta = \arctan \left(\frac{2 K_{\mathrm{I}} K_{\mathrm{II}}}{K_{\mathrm{I}}^2 + K_{\mathrm{II}}^2} \right) \tag{8}$$

Eq. (8) predicts the crack angle following the maximum energy release rate. Fig. 2 shows the plot of θ as function of the ratio $K_{\mathrm{II}}/K_{\mathrm{I}}$.

3.2. Finite element model

Images of extruded starch are meshed considering the conversion of each pixel by an 8-node plane element. The meshing is thus regular and the mesh size corresponds to the resolution of the image. The ANSYS code (ANSYS Inc., Canonsburg, PA, USA) is used for such purpose combined with a self-written program. Plane strain state is assumed within the 2-D linear elastic analysis.

The connectivity of the elements is modified to account for the possibility to propagate a crack in all possible directions (Fig. 3a). Indeed, the elements do not share any of their corresponding nodes but initially all degrees of freedom of coincident nodes are coupled.

Because node decoupling in a regular square grid is limited to three angles (−90°, 0° and 90°), it is performed in a large domain corresponding to the size of the decoupling step (Fig. 3b). In this study, the decoupling domain is restricted to 20 × 20 elements

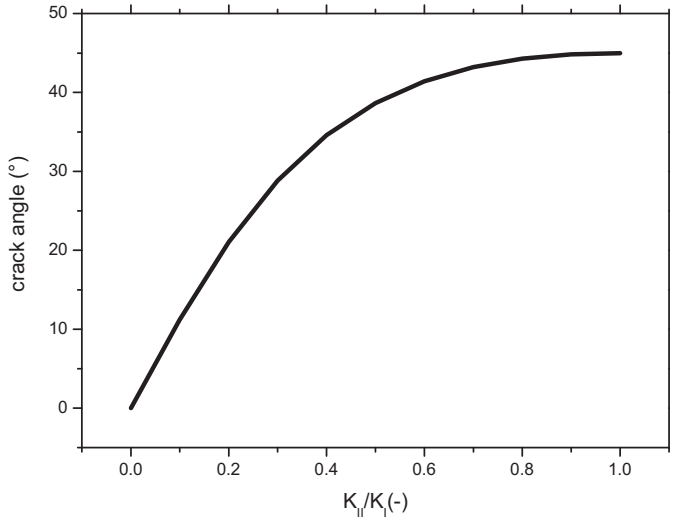

Fig. 2. Prediction of the crack propagation angle as function of the ratio of the stress intensity factors.

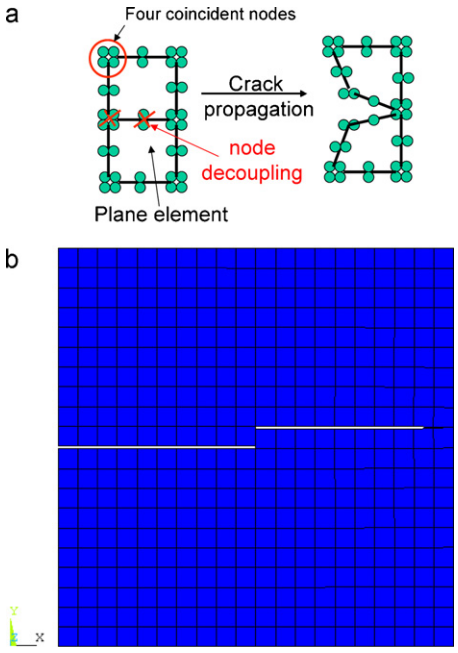

Fig. 3. (a) Crack propagation using node decoupling and (b) node decoupling along a large domain allowing the crack propagation with small angles.

ahead the crack tip, where the physical dimension of this domain depends on the resolution of the images. In our case, the decoupling size is 667 μm for an image resolution of 300 × 300 pixels. The lowest vertical displacement within the decoupling domain predicts crack extension with an angle as small as 2.79°.

The material properties used in our simulation are those corresponding to isotropic elastic materials with a constant Poisson ratio ($\nu = 0.3$). Isotropy is thus assumed at the scale of the individual elements. However, Young's modulus is spatially varied in order to represent the real heterogeneity of starch material. For this purpose, the grey level of each pixel of the image corresponds to an element with a given value of Young's modulus. In such a way, a dark pixel represents an element with a large Young's modulus and vice versa.

The conversion of the grey level into a material property assumes a linear correlation of the form

$$E_i = E_{\max} + \left(\frac{E_{\min} - E_{\max}}{256}\right) n_i \tag{9}$$

where i refers to the pixel index. $E_{\min}$ and $E_{\max}$ are the lower and upper limits for Young's modulus, respectively. n_i is the grey level associated with pixel i.

The linear conversion used in Eq. (9) can be compared to an approximation of the exponential decay of light transmission. Because of the void structure, light attenuation is linear with respect to the depth of penetration in the solid.

The upper bound of the elastic property is fixed to 140 MPa. This value is much less than the elastic modulus of the dense starch material. This value is chosen in accordance with the measured rupture force. The lower bound of the elastic modulus is varied in a large domain (from 140 MPa down to 1 Pa) to account for the sensitivity of the predicted path with regard to the bright regions. Fig. 4 shows an example of image conversion into a finite element model using up to 1397 material models for the carbohydrate polymer. In fact, the same model of isotropic elastic material is used each element is assigned a different value of Young's modulus.

Prior loading, a crack of length comparable to the measured crack size is numerically created by decoupling all those nodes belonging to the crack baseline.

The plate is loaded applying the experimental conditions. All nodes of the bottom line are constrained against displacement in X-direction whereas a structural displacement $-U(t)/2$ is imposed in Y-direction, where t refers to the simulation time. Nodes of the top line are displaced by a positive amount $+U(t)/2$ in Y-direction and the other degrees of freedom are fixed.

The elastic problem is solved using the preconditioned Conjugate Gradient PCG solver. The stress intensity factors are computed thanks to the nodal displacement results. When the imposed displacement reaches the failure value, the crack propagation is

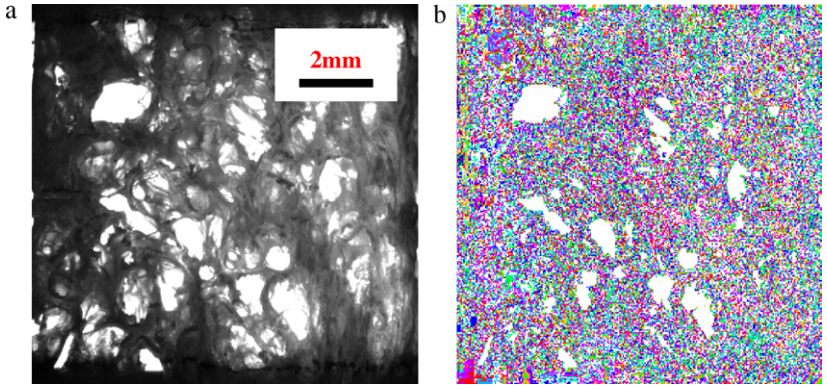

Fig. 4. (a) A typical porous material and (b) the corresponding finite element mesh. Colours associated with elements represent different material properties. ROI area = 100 mm^2.

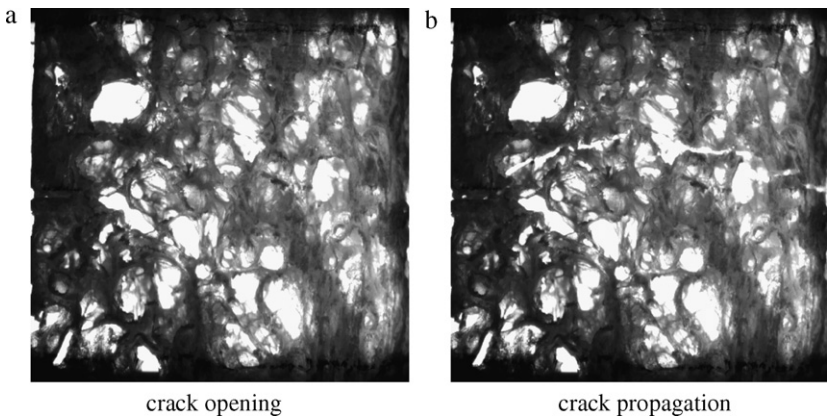

Fig. 5. (a) Largest crack opening corresponding to the peak force and (b) crack propagation leading to brittle rupture of the carbohydrate porous polymer.

started with the implemented criterion [Eq. (8)]. Stress intensity factors are computed in the post-processing thanks to the nodal displacement field. For this purpose, five nodes are used, one corresponding to the crack tip and the nearest two backward nodes for each crack surface.

4. Results and discussion

Fig. 5 shows images of the porous carbohydrate material at different stages. In Fig. 5a, the crack opening is utmost and corresponds to a peak force of about 19 N (failure stress of 1.32 MPa). The loading of the material reveals a slope of about 62 MPa. This value is slightly smaller than Young's modulus of the intact specimen because of the presence of the notch. The crack opening cannot be easily distinguished because the notch intercepts a dense region.

The crack propagation leads to a brittle failure of the material as attested by the abrupt decrease of the force (data not shown). Since the frame rate is fixed to 100 fps, it is not possible to estimate the velocity of the crack growth, or at least, we should say that it is beyond 1 m s^{-1}. The crack trajectory is shown in Fig. 5b. Despite tensile loading, the crack path is jagged. Sudden variations in crack propagation are correlated to the presence of a void structure, because such structure modifies the stress distribution at the cell walls. It is also clear that change in the crack path means the development of a local mixed fracture mode in which shearing has a non-negligible contribution. Jagged crack propagation is not specific to starch foams but it is well observed in various other porous materials (Dillard et al., 2006; Hazenberg, Freeley, Foran, Lee, & Taylor, 2006).

In order to underline the effect of the void structure on the crack trajectory, different values of E_{min} are used. A low bound value is suggested to increase the contrast between dark and bright regions. It is also more realistic with regard to the presence of the void structure. Fig. 6 shows the predicted crack path using the maximum elastic energy release criterion for different values of E_{min}. Note that E_{max} = 140 MPa is constant for all these runs. When $E_{min} = E_{max}$, the material is homogeneous. The crack propagates perpendicular to the loading direction following the opening mode. This result simply indicates that $\theta = 0$ when $K_{II} \to 0$.

The decrease of E_{min}, modifies significantly the crack path. The crack trajectory becomes insensitive to E_{min} below 1 kPa. The computation becomes difficult to perform because of numerical instabilities when $E_{min} \to 0$. Such instabilities are principally due to large deformations associated with elements with small Young's moduli.

The analysis of mesh sensitivity is conducted by resizing the image of the porous carbohydrate material from its original size (300 × 300 pixels) down to 100 × 100 and up to 500 × 500 pixels (Fig. 7a–c). The computation of the crack path with the lowest resolution predicts a significant deviation from the original path (Fig. 7d). This result is not surprising because fewer details appear with subresolutions. For those resolutions larger than 200 × 200 pixels, the path differences become more attenuated. When increasing further more the resolution above the original image size, we do not gain information. However, any pixel in the original image will appear as a homogeneous domain composed of several pixels in the modified image (Fig. 7c). This has a minor, but not negligible, effect on the crack path (Fig. 7d).

Fig. 8a depicts the numerical force–displacement response for one of the test conditions in Fig. 5. Here, the simulation is performed using the original resolution (300 × 300 pixels). The moduli bounds for this case are: E_{min} = 0.001 MPa, E_{max} = 140 MPa. The crack propagation is initiated at a break elongation of 0.21 mm (failure strain of 2.1%). This value is the exactly the elongation at which material rupture is observed in Fig. 5b. The corresponding numerical peak force is about 20 N, which is 5% larger than the experimental failure force. This small deviation is attributed to the selected E_{max} value, as mentioned above.

Fig. 8b depicts the predicted crack path using the maximum elastic energy release criterion. In this figure, evident crack changes can be classified into small and large crack angle variations. Jagged crack extension is related to the heterogeneous distribution of the elastic modulus but its magnitude of variation remains small, i.e., weak contrast of the elastic modulus. Significant path changes are particularly associated with large regions where the elastic modulus is the lowest one. These regions are efficient stress con-

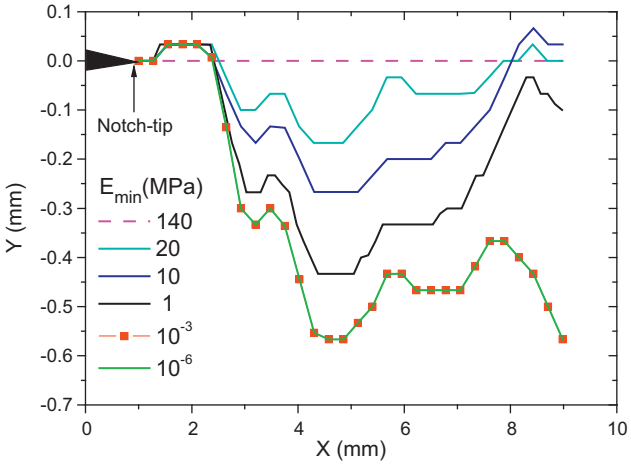

Fig. 6. Comparison between crack paths for different values of E_{min}.

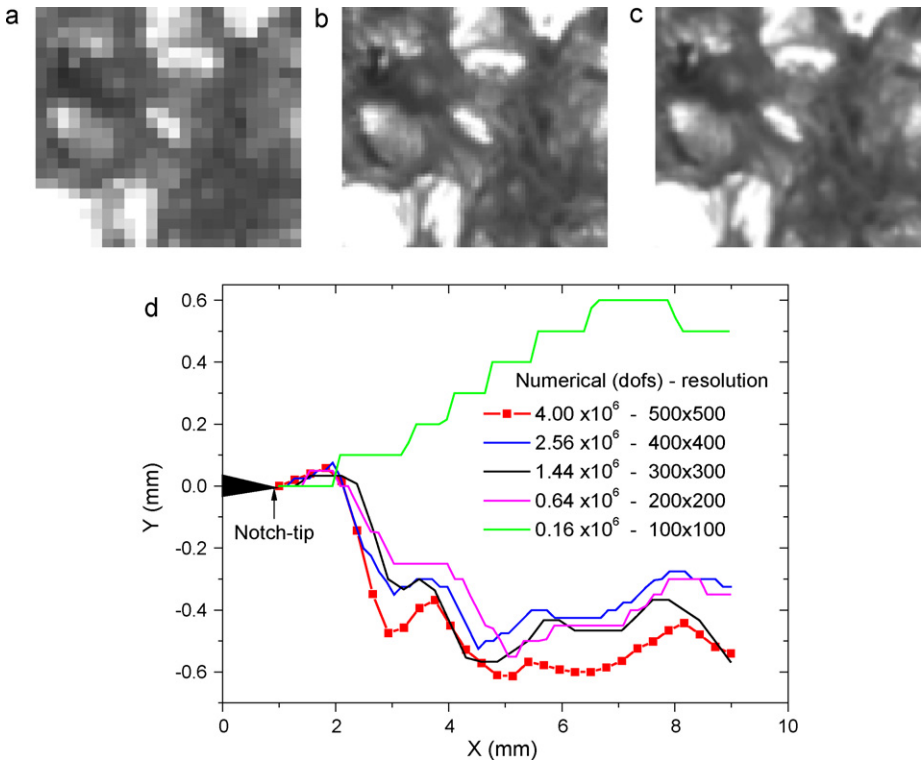

Fig. 7. (a)–(c) The same ROI observed at different resolutions (a) original 300 × 300 pixels, (b) 100 × 100 pixels, (c) 500 × 500 pixels and (d) predicted crack propagation as function of resolution.

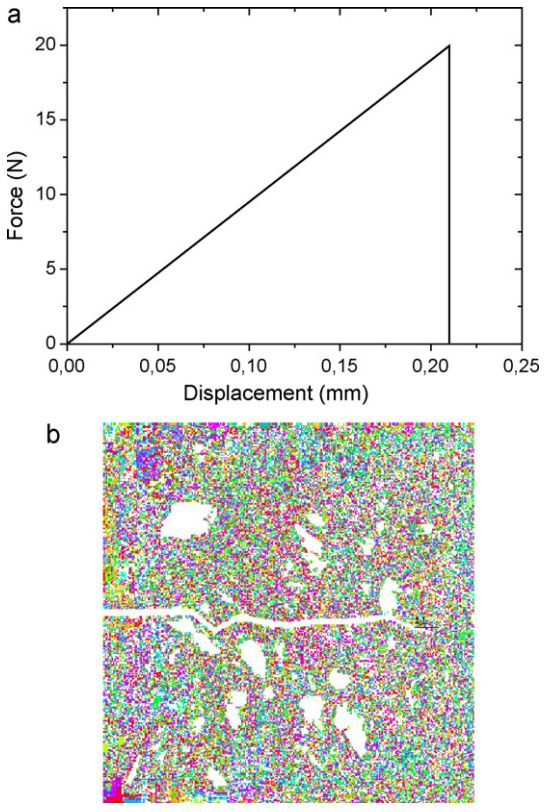

Fig. 8. (a) Predicted force–displacement response using the linear elastic approximation and (b) predicted jagged crack propagation.

centrators because the elastic modulus contrast is utmost. Such contrast makes these regions acting like crack traps. However, the brittle failure of the material indicates that crack traps are not effective in arresting completely the crack progress because elastic energy is still available for the complete failure of the material.

Fig. 9 shows the evolution of the stress distribution in the carbohydrate material as function of crack extension. In Fig. 9a, the stress distribution corresponds to the largest crack opening and thus to the highest stress concentration at the crack tip before propagation. Few decoupling steps ahead, the crack orientation does not change significantly as shown in Fig. 9b. The first significant change of direction in crack propagation corresponds to Fig. 9c, where a significant stress concentration develops downward the crack position. Afterwards, the crack path remains almost normal to the loading direction (Fig. 9d–f) as long as the crack does not encounter stress concentrators.

The analysis of the stress intensity factors reveals that the ratio K_{II}/K_I is significantly affected by the heterogeneous void structure (Fig. 10). K_{II}/K_I is found to vary in a large range from 0.003 up to 0.3. The variation of the crack angle is fully correlated to the ratio K_{II}/K_I as shown in Fig. 10. The jagged character of crack propagation is inferred to the change of the predicted crack angles as a consequence of the strong local mixed mode.

The local mixed mode is strengthened at the first steps of the crack propagation (crack length <4 mm) because of the strong spatial variability of the elastic properties. If we consider the value of K_I at those crack positions, where the opening mode is still predominant (say for example $K_{II}/K_I < 0.01$), K_I fluctuates between 0.12 and 0.33 MPa $m^{0.5}$. For different food items, Vincent (2004) report fracture toughness in the range 0.11–0.13 MPa $m^{0.5}$ (Pérez, Saunders, & Vincent, 2008; Vincent, 2004). For other cellular materials, such as carbonated apatite materials, fracture toughness is 0.14 MPa $m^{0.5}$ (Morgan, Yetkinler, Constantz, & Dauskardt, 1997).

In our case, the fracture toughness can be determined from the critical values of the stress intensity factors in which both K_I and K_{II} are contributors. Indeed, preceding results show that both tension and shearing effects take place in the heterogeneous structure. Such determination of fracture toughness requires different testing configurations that we are not able to proceed with, and in which the critical values of K_I and K_{II} can be separately determined. Numerical attempts have been considered for the determination of the mixed mode crack toughness by changing the loading conditions numerically (Choi & Sankar, 2005), but such studies have unfortunately no experimental validation.

Any combination of K_I and K_{II} in Fig. 10 must lead to an expression that is larger than the fracture toughness. This condition states the unstable crack propagation for our brittle material.

Moreover, few expressions of fracture toughness are available in the case of a mixed mode fracture (Perez, 2004). The reason is that we did not expect shearing effect to develop when measuring the critical value of K_I using tensile loading.

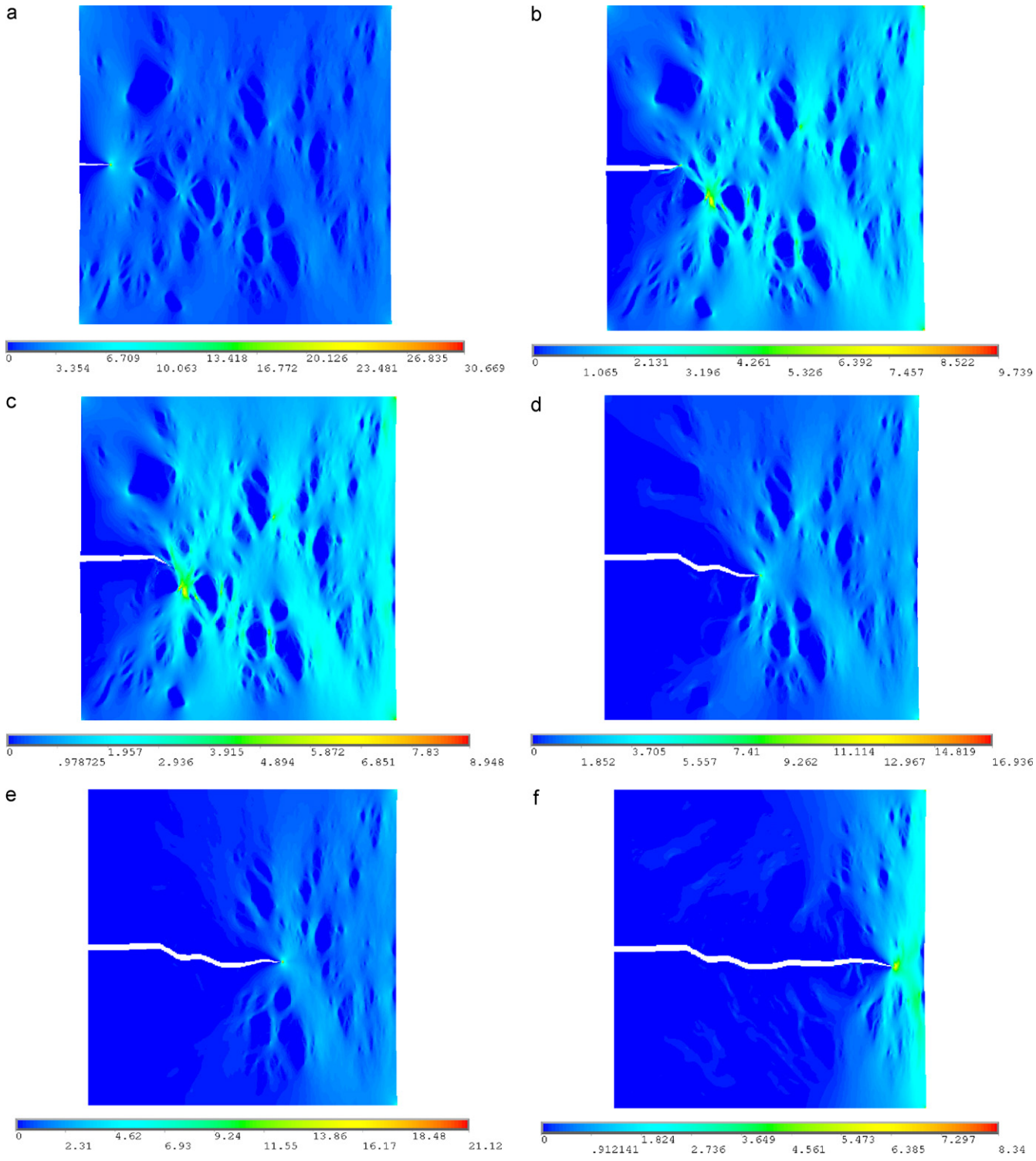

Fig. 9. Principal stress S1 distribution as function of crack extension.

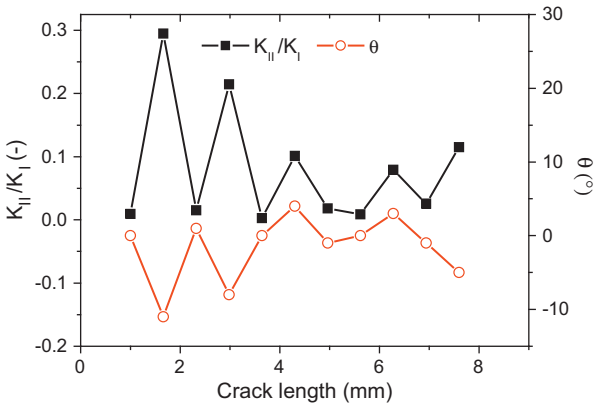

Fig. 10. Ratio of stress intensity factors and predicted crack angle as function of crack position.

The results shown in Fig. 10 well demonstrate that the prediction of the crack path is dependent on how accurate is our description of the void environment of the crack.

In order to describe the effect of such environment on the crack propagation, several porous structures exhibiting different grey level histograms are tested (Fig. 11a). The histogram associated with sample A corresponds to the porous material shown in Fig. 4a. In this case, the pixel frequency of the bright regions is the highest one. Bright regions become less frequent as we move from sample A to sample D.

Fig. 11b exhibits the predicted crack paths for the considered carbohydrate porous materials. The highest jagged path corresponds to material A, exhibiting the largest contrast between the dark and bright regions. In this case, the mixed mode is strengthened because of the stress heterogeneities. Materials C and D are characterised by predicted paths close to the horizontal line, which indicates a predominant opening mode.

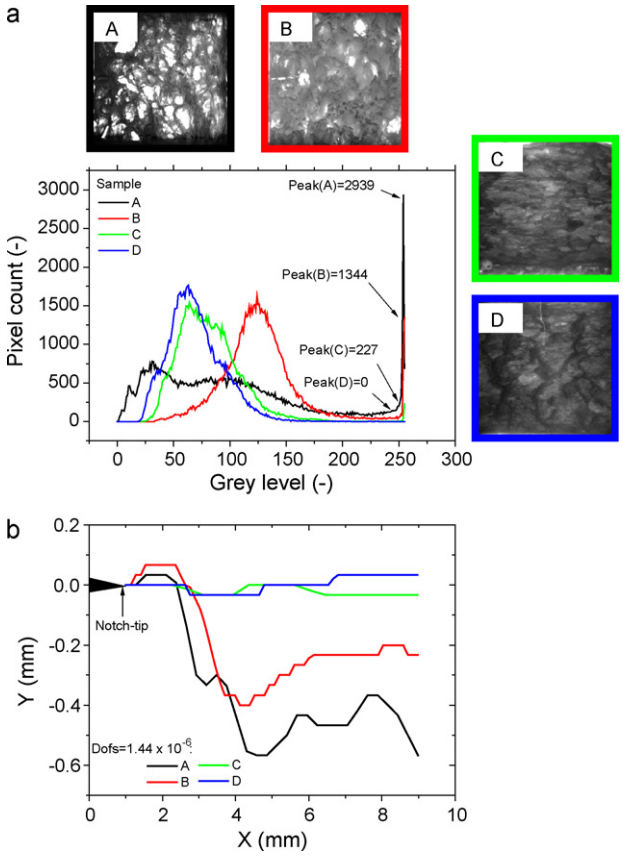

Fig. 11. Effect of void structure: (a) grey-level histograms and (b) the predicted crack paths.

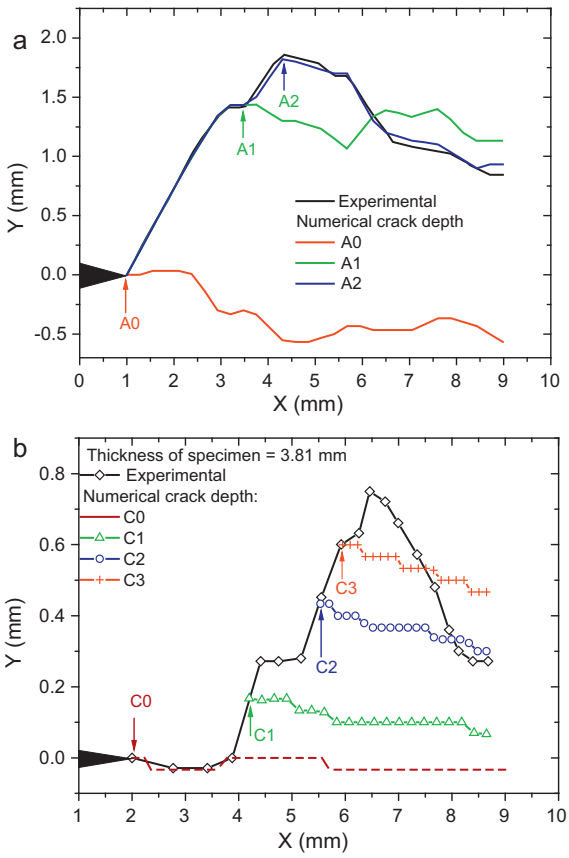

Fig. 12. Comparison between experimental and numerical crack paths for different numerical initial crack positions for two porous carbohydrate materials exhibiting (a) large and (b) low contrast of material properties.

We can confirm, at this stage, that the contrast between dark and bright regions modulates the mixed mode propagation.

When comparing the experimental (Fig. 5b) and numerical (Fig. 9f) crack paths, a significant discrepancy is pointed out. Indeed, the numerical model is not able to predict accurately the first crack propagation increments. The crack trajectory in Fig. 5b remains far above the predicted one. The numerical model fails in predicting significant angle variation in those regions with no evident contrast of material properties. This is precisely the case of the first crack position increments where the presence of a dark region indicates local changes in void structure. Under these circumstances, the true crack propagation can only be approached if 3D crack propagation is considered.

In order to validate our numerical approach, crack propagation is simulated for different crack sizes. The crack tip position corresponds in each run to the real observed position. The purpose here is to increase the initial crack size until adequate matching is found between the numerical and experimental crack trajectories. Fig. 12 compiles the predicted results for two materials exhibiting distinct contrasts A and C. In Fig. 12a are shown the various paths related to sample A. The first configuration (notch-tip A0) corresponds to the case described above in Fig. 9. When extending the crack position to about 3.5 mm (notch-tip A1), there are still differences in crack trajectories. If the crack tip position is increased further (notch-tip A2), the numerical model is able to predict adequately the crack extension.

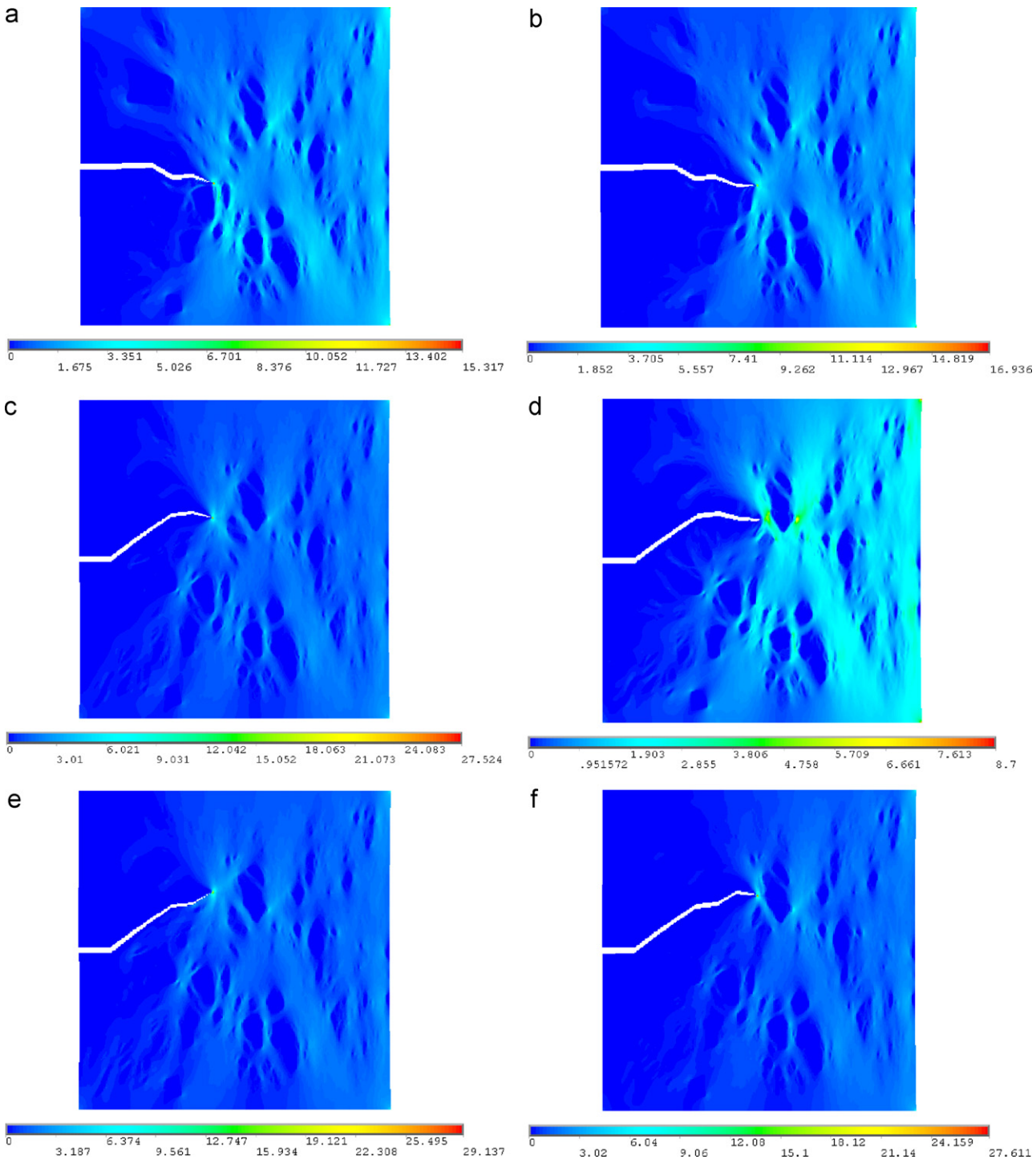

Fig. 13. Evolution of the principal stress S1 distribution at two successive steps: $x = 4.1$ mm for (a), (c) and (e), whereas $x = 4.7$ mm for (b), (d) and (f) for three different notch configurations: (a and b) notch-A0, (c and d) notch-A1 and (e and f) notch-A2.

Fig. 12b shows the path corrections in the case of material C. Because of the low contrast, any correction (notch-tip C1–C3) is not able to predict significant variations in the crack path because stress heterogeneities are not properly described.

Fig. 13 compares the stress distribution evolutions for the crack configurations treated in Fig. 12a. Fig. 13a and b corresponds to the case where no path correction is performed (notch-A). We see for the notch-A1 (Fig. 13c and d) that the simulated crack path propagates towards the bottom periphery of a stress concentrator, where the stress levels are higher. The crack propagates along this periphery, predicting a lower position compared to the experimental path. When correcting the crack position using notch-A2 (Fig. 13e and f), the stress distribution around the heterogeneity is modified. The crack trajectory seems then more accurate and closer to experimental one.

5. Conclusions

- Within the context of linear elastic fracture analysis, a regular meshing is successfully considered for the prediction of small

crack angle variation in a carbohydrate porous material. The angle accuracy depends on the size of the crack increment weighted by the resolution of the image acquisition.

- The description of the porous carbohydrate material in terms of spatial heterogeneous distribution of material properties explains most variations of crack trajectories observed experimentally.
- The development of a strong local mixed mode is dependent on the local material properties contrast. The presence of stress concentrators contributes in changing significantly the crack trajectory; this change is all the more significant as the crack tip is close to these regions with a high stress level.
- The maximum energy release criterion is able to predict the true crack trajectory if the image contrast remains informative of the void structure. A large contrast between bright and dark regions in the porous materials contributes to strengthen the mixed mode.
- The jagged character of crack propagation in the studied starch porous material is correlated to a large variations of the stress intensity factor ratio. This quantity is found to vary in a wide range from 0.003 up to 0.3, whereas K_I changes between 0.12 and 0.33 MPa $m^{0.5}$.

References

Alfaiate, J., Pires, E. B., & Martins, J. A. C. (1997). A finite element analysis of non-prescribed crack propagation in concrete. *Computers & Structures*, *63*(1), 17–26.

Babin, P., Della Valle, G., Dendievel, R., Lourdin, D., & Salvo, L. (2007). X-ray tomography study of the cellular structure of extruded starches and its relations with expansion phenomenon and foam mechanical properties. *Carbohydrate Polymers*, *68*(2), 329–340.

Bazant, Z. P. (1997). Scaling of quasibrittle fracture: Asymptotic analysis. *International Journal of Fracture*, *83*(1), 19–40.

Belytschko, T., Organ, D., & Gerlach, C. (2000). Element-free Galerkin methods for dynamic fracture in concrete. *Computer Methods in Applied Mechanics and Engineering*, *187*(3–4), 385–399.

Cendon, D. A., Galvez, J. C., Elices, M., & Planas, J. (2000). Modelling the fracture of concrete under mixed loading. *International Journal of Fracture*, *103*(3), 293–310.

Chiaia, B., Vervuurt, A., & VanMier, J. G. M. (1997). Lattice model evaluation of progressive failure in disordered particle composites. *Engineering Fracture Mechanics*, *57*(2–3), 301–309.

Choi, S., & Sankar, B. V. (2005). A micromechanical method to predict the fracture toughness of cellular materials. *International Journal of Solids and Structures*, *42*(5–6), 1797–1817.

Cornec, A., Scheider, I., & Schwalbe, K. H. (2003). On the practical application of the cohesive model. *Engineering Fracture Mechanics*, *70*(14), 1963–1987.

Dan, H., & Kohyama, K. (2007). Interactive relationship between the mechanical properties of food and the human response during the first bite. *Archives of Oral Biology*, *52*, 455–464.

Dejak, B., Mlotkowski, A., & Romanowicz, M. (2003). Finite element analysis of stresses in molars during clenching and mastication. *Journal of Prosthetic Dentistry*, *90*(6), 591–597.

Della Valle, G., Colonna, P., Patria, A., & Vergnes, B. (1996). Influence of amylose content on the viscous behaviour of low hydrated molten starches. *Journal of Rheology*, *40*, 347–362.

Della Valle, G., Vergnes, B., Colonna, P., & Patria, A. (1997). Relations between rheological properties of molten starches and their expansion behaviour in extrusion. *Journal of Food Engineering*, *31*(3), 277–295.

Dillard, T., Forest, S., & Ienny, P. (2006). Micromorphic continuum modelling of the deformation and fracture behaviour of nickel foams. *European Journal of Mechanics A: Solids*, *25*(3), 526–549.

Fontanet, I., Davidou, S., Dacremont, C., & LeMeste, M. (1997). Effect of water on the mechanical behaviour of extruded flat bread. *Journal of Cereal Science*, *25*(3), 303–311.

Gao, H. J., & Ji, B. H. (2003). Modeling fracture in nanomaterials via a virtual internal bond method. *Engineering Fracture Mechanics*, *70*(14), 1777–1791.

Gasser, T. C., & Holzapfel, G. A. (2005). Modeling 3D crack propagation in unreinforced concrete using PUFEM. *Computer Methods in Applied Mechanics and Engineering*, *194*(25–26), 2859–2896.

Gdoutos, E. E. (2005). *Fracture mechanics: An introduction*. Dordrecht: Springer.

Geers, M. G. D., de Borst, R., & Peerlings, R. H. J. (2000). Damage and crack modeling in single-edge and double-edge notched concrete beams. *Engineering Fracture Mechanics*, *65*(2–3), 247–261.

Gibson, L. J., & Ashby, M. F. (1997). *Cellular solids*. Cambridge: Pergamon Press Ltd.

Gobron, S., & Chiba, N. (2001). Crack pattern simulation based on 3D surface cellular automata. *Visual Computer*, *17*(5), 287–309.

Guarino, A., Garcimartin, A., & Ciliberto, S. (1998). An experimental test of the critical behaviour of fracture precursors. *European Physical Journal B*, *6*(1), 13–24.

Guy, R. (2001). *Extrusion cooking – Technologies and applications*. Woodhead Publishing.

Hazenberg, J. G., Freeley, M., Foran, E., Lee, T. C., & Taylor, D. (2006). Microdamage: A cell transducing mechanism based on ruptured osteocyte processes. *Journal of Biomechanics*, *39*(11), 2096–2103.

Hellen, T. K., & Blackburn, W. S. (1975). Calculation of stress intensity factors for combined tensile and shear loading. *International Journal of Fracture*, *11*(4), 605–617.

Ho, C.-T., Karwe, M. V., & Kokini, J. L. (1991). *Food extrusion science and technology*. CRC Press.

Ichim, I., Kieser, J. A., & Swain, M. V. (2007). Functional significance of strain distribution in the human mandible under masticatory load: Numerical predictions. *Archives of Oral Biology*, *52*(5), 465–473.

Ingraham, M. D., DeMaria, C. J., Issen, K. A., & Morrison, D. J. (2009). Low cycle fatigue of aluminum foam. *Materials Science and Engineering A: Structural Materials Properties Microstructure and Processing*, *504*(1–2), 150–156.

Jenq, Y. S., & Shah, S. P. (1988). Mixed-mode fracture of concrete. *International Journal of Fracture*, *38*, 123–142.

Kanny, K., Mahfuz, H., Carlsson, L. A., Thomas, T., & Jeelani, S. (2002). Dynamic mechanical analyses and flexural fatigue of PVC foams. *Composite Structures*, *58*(2), 175–183.

Kirby, A. R., & Smith, A. C. (1998). Impact studies on extruded food foams. *Journal of Materials Science*, *23*, 2251–2254.

Lipperman, F., Ryvkin, M., & Fuchs, M. B. (2007a). Fracture toughness of two-dimensional cellular material with periodic microstructure. *International Journal of Fracture*, *146*(4), 279–290.

Lipperman, F., Ryvkin, M., & Fuchs, M. B. (2007b). Nucleation of cracks in two-dimensional periodic cellular materials. *Computational Mechanics*, *39*(2), 127–139.

Lucas, P. W., Prinz, J. F., Agrawal, K. R., & Bruce, I. C. (2002). Food physics and oral physiology. *Food Quality and Preference*, *13*(4), 203–213.

Morel, S., Bouchaud, E., Schmittbuhl, J., & Valentin, G. (2002). *R*-curve behavior and roughness development of fracture surfaces. *International Journal of Fracture*, *114*(4), 307–325.

Morgan, E. F., Yetkinler, D. N., Constantz, B. R., & Dauskardt, R. H. (1997). Mechanical properties of carbonated apatite bone mineral substitute: Strength, fracture and fatigue behaviour. *Journal of Materials Science: Materials in Medicine*, *8*(9), 559–570.

Motz, C, Friedl, O., & Pippan, R. (2005). Fatigue crack propagation in cellular metals. *International Journal of Fatigue*, *27*(10–12), 1571–1581.

Okada, A., Honma, M., Nomura, S., & Yamada, Y. (2007). Oral behavior from food intake until terminal swallow. *Physiology & Behavior*, *90*, 172–179.

Pérez, F. J. R., Saunders, D., & Vincent, J. F. V. (2008). Mechanical tests on crispy & crunchy foods. In *Crispy cracks symposium* Wageningen, The Netherlands.

Perez, N. (2004). *Fracture mechanics*. Boston: Kluwer Academic Publishers.

Prado, E. P., & van Mier, J. G. M. (2003). Effect of particle structure on mode I fracture process in concrete. *Engineering Fracture Mechanics*, *70*(14), 1793–1807.

Primo-Martin, C., de Beukelaer, H., Hamer, R. J., & van Vliet, T. (2008). Fracture behaviour of bread crust: Effect of bread cooling conditions. *Journal of Food Engineering*, *89*(3), 285–290.

Reina, J. M., Garcıa-Aznar, J. M., Domınguez, J., & Doblare, M. (2007). Numerical estimation of bone density and elastic constants distribution in a human mandible. *Journal of Biomechanics*, *40*, 828–836.

Rice, J. R. (1968). A path independent integral and approximate analysis of strain concentration by notches and cracks. *Journal of Applied Mechanics*, *35*(2), 379–386.

Rohrle, O., & Pullan, A. J. (2007). Three-dimensional finite element modelling of muscle forces during mastication. *Journal of Biomechanics*, *40*(15), 3363–3372.

Ryvkin, M., Fuchs, M. B., Lipperman, F., & Kucherov, L. (2004). Fracture analysis of materials with periodic microstructure by the representative cell method. *International Journal of Fracture*, *128*(1–4), 215–221.

Sandoval, A. J., Chaunier, L., Courcoux, P., & Della Valle, G. (2008). Bulk mechanical behavior of commercial particle food foams. *Journal of Texture Studies*, *39*(4), 405–425.

Saouma, V. E. (2008). Lecture notes. In *Fracture mechanics*. University of Colorado.

Schlangen, E., & Garboczi, E. J. (1996). New method for simulating fracture using an elastically uniform random geometry lattice. *International Journal of Engineering Science*, *34*(10), 1131–1144.

Schlangen, E., & Garboczi, E. J. (1997). Fracture simulations of concrete using lattice models: Computational aspects. *Engineering Fracture Mechanics*, *57*(2–3), 319–332.

Schmidt, I., & Fleck, N. A. (2001). Ductile fracture of two-dimensional cellular structures. *International Journal of Fracture*, *111*(4), 327–342.

Taylor, D., Hazenberg, J. G., & Lee, T. C. (2003). The cellular transducer in damage-stimulated bone remodelling: A theoretical investigation using fracture mechanics. *Journal of Theoretical Biology*, *225*(1), 65–75.

Thuvander, F., Jernkvist, L. O., & Gunnars, J. (2000). Influence of repetitive stiffness variation on crack growth behaviour in wood. *Journal of Materials Science*, *35*(24), 6259–6266.

Turker, K. S., Sowman, P. F., Tuncer, M., Tucker, K. J., & Brinkworth, R. S. A. (2007). The role of periodontal mechanoreceptors in mastication. *Archives of Oral Biology*, *52*, 361–364.

Vendra, L., Neville, B., & Rabiei, A. (2009). Fatigue in aluminum–steel and steel–steel composite foams. *Materials Science and Engineering A: Structural Materials Properties Microstructure and Processing*, *517*(1–2), 146–153.

Vincent, J. F. V. (2004). Application of fracture mechanics to the texture of food. *Engineering Failure Analysis*, *11*(5), 695–704.

Voon, F. C. T., Lucas, P. W., Chew, K. L., & Luke, D. A. (1986). A simulation approach to understanding the masticatory process. *Journal of Theoretical Biology*, *119*(3), 251–262.

Wilkinson, C., Dijksterhuis, G. B., & Minekusy, M. (2000). From food structure to texture. *Trends in Food Science and Technology*, *11*, 442–450.

Wittel, F. K., Dill-Langer, G., & Kroplin, B. H. (2005). Modeling of damage evolution in soft-wood perpendicular to grain by means of a discrete element approach. *Computational Materials Science*, *32*(3–4), 594–603.

Wu, Z. S., & Yin, J. (2003). Fracturing behaviors of FRP-strengthened concrete structures. *Engineering Fracture Mechanics*, *70*(10), 1339–1355.

Xu, W. L., Kuhnert, L., Foster, K., Bronlund, J., Potgieter, J., & Diegel, O. (2007). Object-oriented knowledge representation and discovery of human chewing behaviours. *Engineering Applications of Artificial Intelligence*, *20*(7), 1000–1012.

Zhu, W. C., & Tang, C. A. (2004). Micromechanical model for simulating the fracture process of rock. *Rock Mechanics and Rock Engineering*, *37*(1), 25–56.